ROYAL SOCIETY OF CHEMISTRY

EDGE ARTICLE

Enantioselective synthesis of α-aryl α-hydrazino phosphonates†

Saúl Alberca, [ID] [a] Javier Romero-Parra,[b] Israel Fernández, [ID] *[c] Rosario Fernández, [ID] *[a] José M. Lassaletta [ID] *[d] and David Monge [ID] *[a]

Catalysts generated *in situ* by the combination of pyridine–hydrazone *N,N*-ligands and Pd(TFA)$_2$ have been applied to the addition of arylboronic acids to formylphosphonate-derived hydrazones, yielding α-aryl α-hydrazino phosphonates in excellent enantioselectivities (96 → 99% ee). Subsequent removal of the benzyloxycarbonyl (Cbz) *N*-protecting group afforded key building blocks en route to appealing artificial peptides, herbicides and antitumoral derivatives. Experimental and computational data support a stereochemical model based on aryl-palladium intermediates in which the phosphono hydrazone coordinates in its *Z*-configuration, maximizing the interactions between the substrate and the pyridine–hydrazone ligand.

Introduction

Phosphonic acids, phosphonates and their derivatives are involved in numerous biological processes.[1] In drug design, the phosphonate group is often used as a bioisostere of carboxylate. For instance, various phosphonate analogues of known neuraminidase inhibitors exhibit improved pharmacokinetic properties to treat influenza infection.[2] α-Amino phosphonic acid derivatives, acting as amino acid mimics, are known to exhibit important biological activities such as antifungal,[3] antibacterial,[4] antioxidant,[5] anti-Alzheimer,[6] antiviral,[7] and anticancer activities,[8] among others.[9] Additionally, non-proteogenic α-hydrazino phosphonic acid derivatives, in which intramolecular H-bonds (hydrazino turns)[10] might modify their biological activities, have emerged as promising targets in medicinal chemistry. In particular, α-hydrazinophosphonate oxadiazoles **I**,[11] isatin derivatives **II**[12] and hydrazide **III**[4a] have been reported to exhibit promising activities against different types of cancer (**I** and **II**) and antimicrobial activity against *K. Pneumonia* (**III**)

(Fig. 1). Moreover, α-aryl α-hydrazino phosphonates are also the key precursors of pyrazoles **IV**[13,14] which have been shown to have a potent herbicidal activity.

To the best of our knowledge, however, enantiomerically pure forms of these molecules have never been evaluated nor even synthesized. To date, existing routes for the synthesis of α-hydrazino phosphonates-related derivatives rely on various strategies such as metal-catalyzed electrophilic amination of β-keto phosphonates with azodicarboxylates (α-alkyl substitution),[15] cycloaddition reactions employing α-(diazomethyl)-phosphonate for the construction of cyclic heterocycles[16] and asymmetric hydrophosphonylation reaction of azomethine imines to afford cyclic hydrazides (C–P bond forming reaction).[17] Other approaches based on enantioselective reactions involving phosphono hydrazones remain underdeveloped. For instance, Pd[II]-catalyzed enantioselective hydrogenation of α-hydrazono phosphonates has been shown to provide α-aryl α-hydrazine phosphonates.[18] However, the resulting products lack removable *N*-protecting groups necessary to access versatile free hydrazines. Hence, subsequent transformation into α-amino phosphonates by reductive N–N bond cleavage was performed

[a]Departamento de Química Orgánica, Facultad de Química, Universidad de Sevilla and Centro de Innovación en Química Avanzada (ORFEO-CINQA), C/ Prof. García González, 1, 41012 Sevilla, Spain. E-mail: ffernan@us.es; dmonge@us.es

[b]Departamento de Química Orgánica y Fisicoquímica, Facultad de Ciencias Químicas y Farmacéuticas, Universidad de Chile, Olivos 1007, Santiago 8380544, Chile

[c]Departamento de Química Orgánica I and Centro de Innovación en Química Avanzada (ORFEO-CINQA), Facultad de Ciencias Químicas, Universidad Complutense de Madrid, 28040, Madrid, Spain. E-mail: israel@quim.ucm.es

[d]Instituto Investigaciones Químicas (CSIC-US) and Centro de Innovación en Química Avanzada (ORFEO-CINQA), C/ Américo Vespucio 49, 41092 Sevilla, Spain. E-mail: jmlassa@iiq.csic.es

† Electronic supplementary information (ESI) available: Additional optimization results, full experimental procedures, characterization data, NMR spectra for new compounds, HPLC traces, detailed DFT calculations. See DOI: https://doi.org/10.1039/d4sc00822g
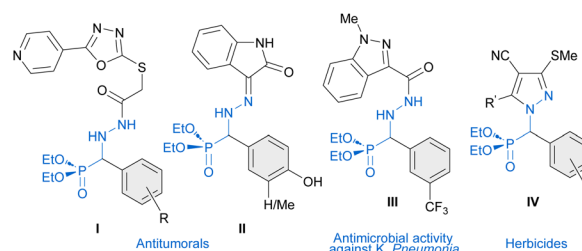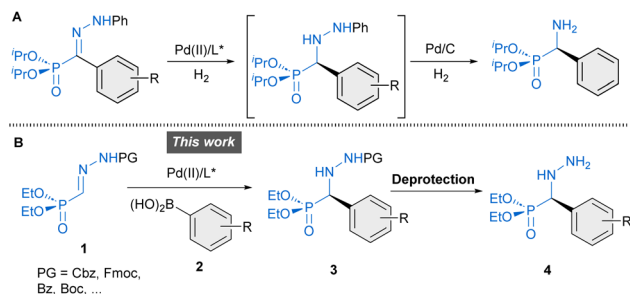

Fig. 1 Biologically active molecules derived from α-aryl α-hydrazino phosphonates.

Scheme 1 Enantioselective transformations of phosphono hydrazones towards α-aryl α-amino phosphonates (A) and α-aryl α-hydrazino phosphonates (B, this work).

Table 1 Optimization of reaction conditions[a]

Entry	1	L*	3	Conv. (%)[b]	ee (%)[c]
1	(E)-1A	L1	(S)-3Aa	20	33
2	(E)-1A	L2	(S)-3Aa	46	rac
3	(E)-1A	L3	(R)-3Aa	70	94
4	(E)-1A	L4	(R)-3Aa	52	97
5	(E)-1A	L5	(R)-3Aa	84	99
6	(E)-1A	L6	(R)-3Aa	85	93
7	(Z)-1A	L5	(R)-3Aa	86	98
8[d]	(E)-1A	L5	(R)-3Aa	68	98

[a] Reactions at 0.1 mmol scale. Reaction time: 24 hours. [b] Estimated by ^{31}P-NMR. [c] Determined by HPLC on chiral stationary phases. [d] Performed with 2,4,6-triphenylboroxine (0.05 mmol).

instead (Scheme 1A). To overcome these limitations, we have developed diverse enantioselective arylation reactions of related hydrazones containing readily removable protecting groups (Cbz, Fmoc, etc.), which allowed the access to free hydrazino building blocks in enantiomerically enriched forms.[19] In this article, we present a straightforward approach to α-aryl α-hydrazino phosphonates **4** based on Pd^{II}-catalyzed enantioselective addition of aryl boronic acids to α-hydrazono phosphonates **1** (C–C bond-forming reaction), enabling, for the first time, a convenient access to this type of molecules in enantioselective fashion (Scheme 1B). In addition, Density Functional Theory (DFT) calculations were carried out to understand the factors leading to the excellent enantioselectivity of the transformation.

Results and discussion

Preliminary experiments were conducted with benzyloxycarbonyl Cbz-protected hydrazone **1A** and phenylboronic acid (**2a**) as model reagents. A preliminary screening of palladium complexes [prepared *in situ* from bipyridine (bipy) and different Pd^{II} sources] and conditions served to identify bipy/Pd(TFA)$_2$ as the most efficient achiral catalyst and dichloroethane (DCE) at 60 °C as the best reaction medium.† Then, diverse chiral pyridine-oxazolines[20] and pyridine–hydrazones[21] were evaluated as chiral N,N′ ligands for the enantioselective version of the reaction (Table 1). To our delight, the use of pyridine–hydrazone **L3** provided, after 24 hours, the desired adduct **3Aa** with 70% conversion and 94% ee (entry 3), clearly outperforming the results obtained with commercially available pyridine-oxazolines **L1** and **L2** (entries 1 and 2). The (2S,5S)-2,5-diphenylpyrrolidine unit was retained as optimal chiral scaffold and the influence of the substituent attached to the C5 of the pyridine ring was also investigated. The presence of 3,5-bis-trifluoromethylphenyl group (R = Ar^F) led to a diminished catalytic activity (entry 4). On the contrary, ligand **L5** bearing a methyl carboxylate group (R = CO$_2$Me) afforded **3Aa** in 84% conversion and excellent enantiocontrol (99% ee). Finally, the incorporation of (2S,5S)-2,5-di-(3,5-bis-trifluoromethylphenyl) pyrrolidine in ligand **L6** led to a slightly lower enantioselectivity (93% ee) compared to ligands **L3–L5**, with the same level of conversion than **L5** (entry 6). Interestingly, a similar

result and the same stereochemical outcome were observed in an additional experiment employing the *cis* isomer (Z)-**1A** (entry 7), suggesting the participation of a common Pd^{II}-intermediate. During the scaling-up, we observed that the eventual presence of boronic acid anhydrides, normally present in commercial boronic acids, might be the origin of some erratic results. In fact, a control experiment revealed that reactivity dropped when 2,4,6-triphenylboroxine (**2a′**) was used instead of phenyl boronic acid (entry 8). Therefore, the remaining optimization was performed employing **2a** after purification by filtration through a short pad of silica gel.† Under optimal conditions, the model reaction on a 0.2 mmol scale required a longer reaction time (36 hours), affording (R)-**3Aa** in 66% yield and 99% ee (Scheme 2). The scope and limitations of the reaction were then explored. First, modifications of hydrazone reagent **1** were investigated. Other N-protecting groups such as 9-fluorenylmethoxycarbonyl (Fmoc) and benzoyl (Bz) were well tolerated, affording (R)-**3Ba** and (R)-**3Ca** in good yields (68–69%) and 98% ee in both cases. Interestingly, a *tert*-butoxycarbonyl (Boc) group in hydrazone **1D** hampered the process, giving **3Da** with high enantioselectivity, albeit in low yield (17%). Overall, these results suggest that the aromatic scaffolds in N-carbamoyl/benzyl groups might stabilize the reactive intermediates through additional π···π interactions, although a more significant steric repulsion by the Boc group cannot be disregarded. Modification of the phosphonate moiety was also investigated. The dimethyl derivative (**1E**) afforded (R)-**3Ea** in 62% yield and slightly lower enantioselectivity (96% ee). Next, Cbz protected hydrazono phosphonate (E)-**1A** was made to react with a variety of arylboronic acids **2a–o** to afford α-aryl α-hydrazide phosphonates **3** in variable yields (30–92%) and excellent enantioselectivities (96–99% ee) in all cases (Scheme 2). Mono-substituted electron-rich aryl boronic acids [**2b**: p-Me–C$_6$H$_4$–B(OH)$_2$, **2c**: p-MeO–C$_6$H$_4$–B(OH)$_2$, **2d**: p-
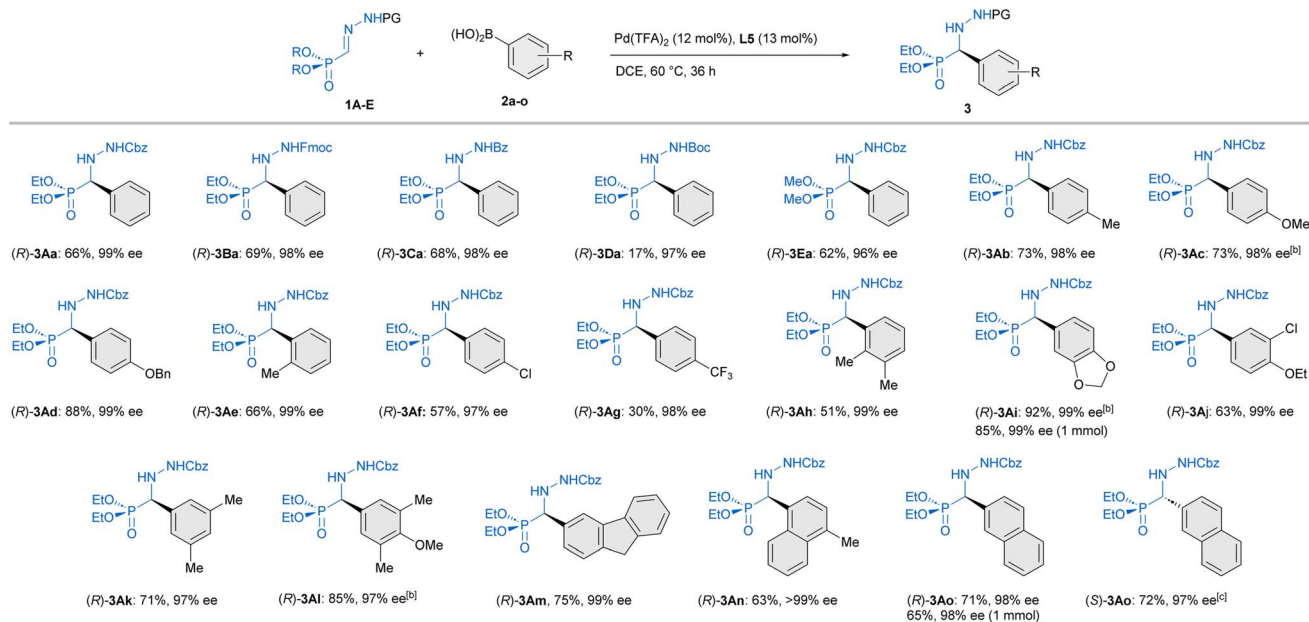
Scheme 2 Scope of the reaction. Yields of isolated products after column chromatography. Enantiomeric excesses were determined by HPLC on chiral stationary phases [a] Reactions performed at 0.2 mmol scale. [b] Reaction time: 20 h. [c] (S)-**3Ao** was synthesized employing *ent*-**L5**.

BnO–C$_6$H$_4$–B(OH)$_2$ and **2e**: *o*-Me–C$_6$H$_4$–B(OH)$_2$] were suitable reagents, whereas electron-poor boronic acids [**2f**: *p*-Cl–C$_6$H$_4$–B(OH)$_2$, **2g**: *p*-CF$_3$–C$_6$H$_4$–B(OH)$_2$] reacted more slowly, leading to side reactions such as homo-coupling and protodeboronation. Hence, portionwise addition of these reagents was required for the synthesis of (*R*)-**3Af** and (*R*)-**3Ag** in 57 and 30% yield, respectively. Di- [*ortho/meta* (**2h**), *meta/para* (**2i** and **2j**), *meta/meta* (**2k**)] and tri-substituted (**2l**) aryl boronic acids afforded **3Ah–3Al** in good yields (51–92%) and high enantioselectivities (97–99% ee). Additionally, aryl boronic acids bearing extended rings, such as **2m** and naphthyl scaffolds (**2n** and **2o**) gave essentially enantiopure α-hydrazide phosphonates **3Am–3Ao** (98 → 99% ee). Finally, heteroaryl (3-furanyl and 3-thienyl) boronic acids and aryl boronic acids **2** containing nitrogenous functional groups (R = *p*-dimethylamino and R = *p*-acetamido) as well as a vinyl chain (R = CH=CH$_2$) were unproductive reagents for this transformation. In a couple of representative examples (**3Ai** and **3Ao**), the reaction could be scaled to 1 mmol without significant loss in yield or enantioselectivity. The absolute *R* configuration of products **3Aa**, **3Ba** and **3Da** was assigned by chemical correlation.† Assuming a uniform reaction pathway, the absolute configurations of all other α-aryl α-hydrazide phosphonates **3** were assigned by analogy.

Experimental data, such as the observed stereoconvergence and the detection of both isomers in independent reactions starting from (*E*)-**1A** or (*Z*)-**1A**, suggest that the reaction proceeds under Curtin-Hammett control[22] with a relatively fast interconversion of stereoisomers. It is known that depending on subtle structure variations and reaction conditions, such as heating in the presence of acids, these types of *E* and *Z* isomers might equilibrate.[23] In order to shed light over reaction mechanism, ^{31}P-NMR was used for monitoring the *E/Z* isomerization

process at 60 °C, showing that the interconversion is facilitated either by the presence of phenyl boronic acid (1 equiv) (*E/Z* from 100 : 0 to 75 : 25, after 1 hour) or catalytic amounts (12 mol%) of Pd(TFA)$_2$ (*E/Z* from 100 : 0 to 75 : 25, after 5 h). Next, the reactions starting from (*E*)-**1A** or (*Z*)-**1A** were also independently
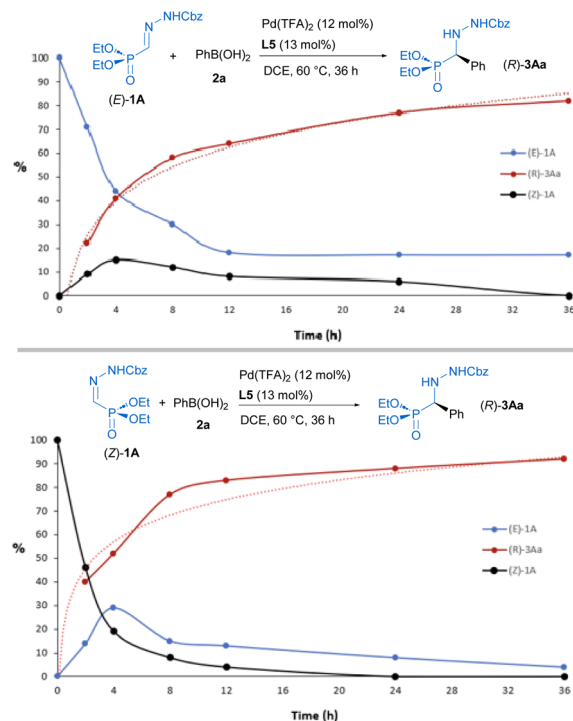

Fig. 2 Progression of ratios (%) of (*E*)-**1A** (in blue), (*Z*)-**1A** (in black) and (*R*)-**3Aa** (in red) under catalytic conditions (0.2 mmol). Estimated by ^{31}P-NMR. (Top) starting from (*E*)-**1A**. (Bottom) starting from (*Z*)-**1A**.

monitored and their profiles over time comparatively analyzed (Fig. 2).

Coexistence of both isomers during the process suggests a relatively low E/Z interconversion barrier upon reaction conditions. Nevertheless, it is observed that conversion to product (R)-**3Aa** over time remains higher when starting from the (Z)-isomer, supporting a preferred pathway through palladium complexes involving (Z)-**1A**. Density Functional Theory (DFT) calculations were carried out to understand the origin of the observed complete enantioselectivity of the transformation. According to a previous report on related Pd^{II}-catalyzed asymmetric addition of arylboronic acids to cyclic N-sulfonyl ketimine esters,[20e] the transformation involves the initial phenyl transfer from the boronic acid to the active palladium(II) catalyst, coordination of the hydrazone followed by intramolecular C–C bond formation, protonation and concomitant regeneration of the catalyst (see Fig. S1 in the ESI† for the computed entire reaction profile). Therefore, the intramolecular C–C bond formation constitutes the enantiodetermining step of the transformation. We consequently focused on this particular reaction step for our system, starting from the initially formed intermediated **INT1**, where the reactive phenyl group and the hydrazone **1E** (Z or E) are directly attached to the Pd^{II}-center bearing the chiral ligand **L5**. Our calculations indicate, not surprisingly, that **INT1**(Z) is 1.8 kcal mol^{-1} more stable than its isomer **INT1**(E), which is mainly due to the occurrence of a stabilizing P=O···HN intramolecular hydrogen bond (see Fig. 3). Despite this, after a conformational search, we were able to locate two transition states for each isomer associated with the formation of the key C–C bond leading to the R (**TS^R**) or S (**TS^E**) enantiomers (with respect to the newly formed stereocenter, Fig. 3). Regardless of the initial intermediate, the formation of the R-enantiomer is favored from both kinetic and thermodynamical points of view, which agrees with the complete enantioselectivity towards the (**R**)-**3** reaction product observed experimentally (see above). From the data in Fig. 3, it is clear that the pathway involving the transition state **TS^R**(Z) becomes the preferred one, leading to the

intermediate **INT2^R**(Z) in an exergonic transformation ($\Delta G_R = -2.3$ kcal mol^{-1} with an activation barrier of only 13.8 kcal mol^{-1}), consistent with the reaction conditions used in the experiments. Remarkably, there is an energy gap of 7.3 kcal mol^{-1} with **TS^S**(E), fully consistent with the almost complete enantioselectivity observed systematically in the experiments. The remarkable stability of **TS^R**(Z) can be initially ascribed, according to the NCIPlot method,[24] to the existence of stabilizing noncovalent $\pi\cdots\pi$ interactions between the phenyl group of CBz and the pyridine fragment of the chiral ligand, along with CH$\cdots\pi$ interactions involving the azomethine proton (N=C)H of the hydrazone and a phenyl group of the pyrrolidine moiety in **L5** (see Fig. 4, left). As these interactions are absent in the analogous transition state leading to the S-isomer, it is not surprising that **TS^R**(Z) is by far the most stable saddle point. More quantitative insight into the factors favoring the pathway involving **TS^R** can be gained by applying the Activation Strain Model (ASM) of reactivity.[25] This analysis involves decomposing the electronic energy (ΔE) into two terms: the strain (ΔE_{strain}) resulting from the distortion of the individual reactants and the interaction (ΔE_{int}) between the deformed reactants along the reaction coordinate, defined in this case by the formation of the key C$\cdots$C bond. As this particular transformation occurs intramolecularly, the fragments, $i.e.$, the hydrazone and the [Pd–Ph]$^+$ complex, were referred to the geometry they adopt in the initial intermediate **INT1**(Z), constituting therefore the zero level of the different ASM terms. Fig. 4a (right) shows the corresponding activation strain diagrams (ASDs) computed for the R and S pathways starting from **INT1**(Z) up to the respective transition states. From the data in Fig. 4a, it becomes clear that the process leading to the R-isomer benefits from a less destabilizing distortion (measured by the $\Delta\Delta E_{strain}$ curve) and, particularly, from a much stronger interaction between the hydrazone and the palladium complex along the entire reaction coordinate. Indeed, whereas the $\Delta\Delta E_{int}$ term becomes clearly stabilizing ($i.e.$, negative) in the proximity of **TS^R**(Z), the situation sharply contrasts in the S-pathway, where the change in the interaction from the
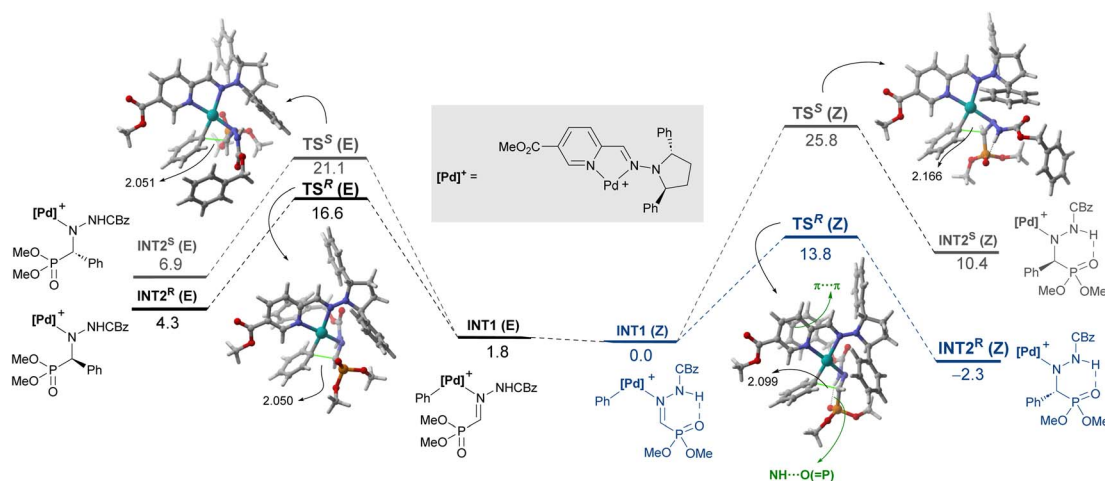

Fig. 3 Computed reaction profile for the key enantiodetermining step from intermediates INT1. Relative free energies (ΔG, at 333 K) and bond distances are given in kcal mol^{-1} and angstroms, respectively.
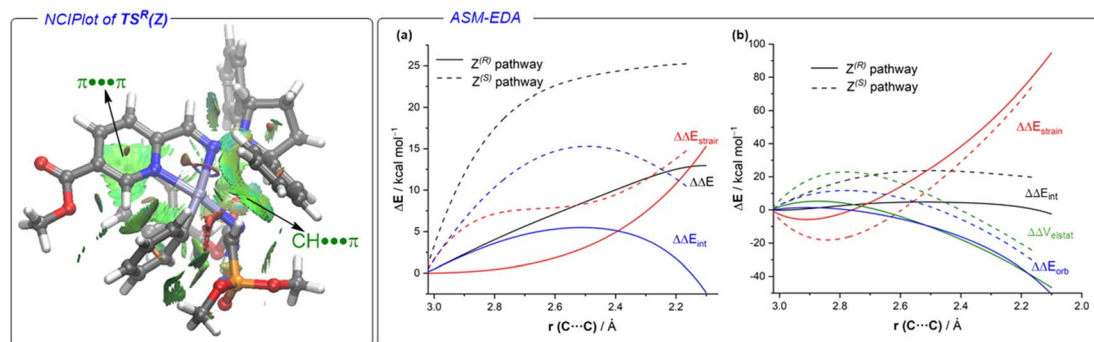
Fig. 4 (Left): Contour plots of the reduced density gradient isosurfaces (density cutoff of 0.04 a.u.) for $TS^R(Z)$. The greenish surfaces indicate attractive non-covalent interactions (computed at the PCM(dichloroethane)-M06L/def2-SVP level). (Right): (a) comparative activation strain analyses (PCM(dichloroethane)-M06L/def2-SVP level) and (b) energy decomposition analyses (ZORA-M06L/DZP//PCM(dichloroethane)-M06L/def2-SVP level) of the key enantiodetermining step projected onto the C···C bond-forming distance and involving the R (solid lines) and S (dotted lines) pathways.

initial intermediate **INT1(Z)** becomes destabilizing. The reasons behind the stronger interaction computed for the R-pathway were further analyzed with the help of the Energy Decomposition Analysis (EDA) method,[26] which involves decomposing the ΔE_{int} into three chemically meaningful terms: classical electrostatic interaction (ΔV_{elstat}), Pauli repulsion between closed-shell orbitals, responsible for steric repulsion, and stabilizing orbital attractions ($\Delta\Delta E_{orb}$). As graphically depicted in Fig. 4b, which shows the evolution of the EDA terms along the reaction coordinate and referred again to the starting intermediate, it becomes clear that the stronger interaction computed for the R-pathway does not result from the $\Delta\Delta E_{Pauli}$ repulsion term, which is actually less destabilizing for the S-pathway (mainly due to the longer C···C bond-forming distance in $TS^S(Z)$ and the closer proximity of the CBz group to the chiral ligand in the Z-pathway), but exclusively from much stronger electrostatic and orbital interactions (in a nearly identical extent) between the palladium complex and the hydrazone fragments, once again along the entire reaction coordinate, and particularly, at the transition state region. Therefore, it can be concluded that the (practically exclusive) formation of the R-enantiomer finds its origin mainly in the electrostatic, orbital and non-covalent interactions between the palladium-complex and hydrazone substrate, which are maximized in the favored Z(R) reaction pathway.

Finally, to further demonstrate the usefulness of this transformation, different derivatization reactions were carried out. N'-Cbz-protected α-aryl α-hydrazino phosphonates **3** are versatile building blocks for accessing compounds with potential applications in diverse fields (Scheme 3). Applying standard hydrogenolysis [Pd(C)/H₂ (1 atm), rt], the benzyloxycarbonyl group (Cbz) of (R)-**3A** was efficiently removed to afford the corresponding hydrazino phosphonates, as exemplified in the synthesis of (R)-**4i** which was isolated as its hydrochloride salt in 90% yield and 99% ee. Additionally, the 2-nathphyl derivative (R)-**3Ao** reacted with 2-[bis(methylthio)-methylene]malononitrile to afford pyrazole (R)-**5o** (a representative of products **III** in Fig. 1) in good yield. Moreover, the introduction of amino acids by N(2) couplings from (R)-**3Aa** and (R)-**3Ai** was performed in one-pot fashion. Thus, hydrogenolysis in the presence of the N-Boc-L-

phenyl alanine anhydride [(N-Boc-Phe)₂O] afforded N(2)-hydrazides (R)-**6a** and (R)-**6i** in good overall yields (56–69%, two steps, only one chromatographic purification), without erosion of the enantioselectivity (96 : 4–99 : 1 dr).

Subsequent deprotection of the Boc group in (R)-**6i** allowed the isolation of (R)-**7i** in 90% yield, emphasizing the potential of hybrid amino acid/hydrazide phosphonates as versatile intermediates for the synthesis of artificial peptides. Finally, the synthesis of enantiopure anti-cancer α-aryl α-hydrazino phosphonates (compounds **I** in Fig. 1) was accomplished by reaction of deprotected hydrazines with bromoacetic anhydride to yield
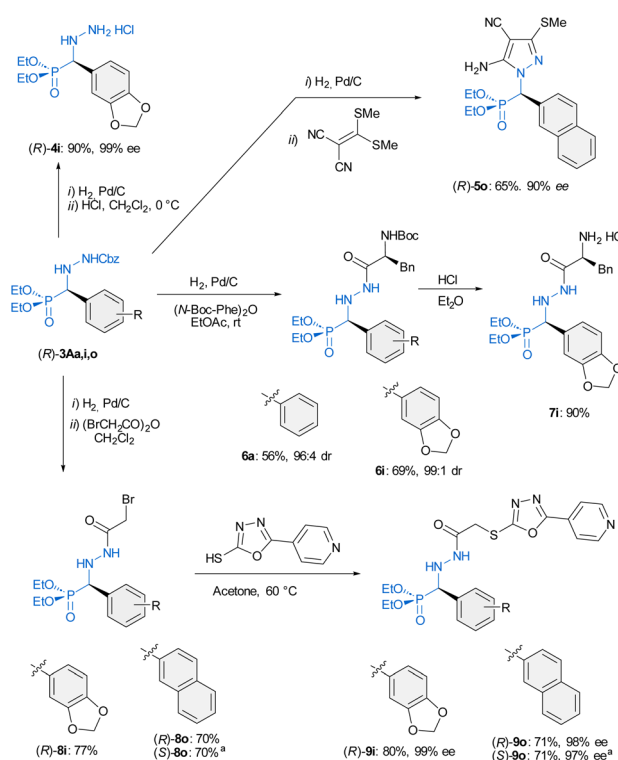
Scheme 3 Transformations of adducts **3** into appealing targets. [a]From (S)-**3Ao**.

key intermediates (*R*)-**8i** and (*R*)-**8o** followed by reaction with commercially available 5-(pyridine-4-yl)-1,3,4-oxadiazole-2-thiol in acetone at 60 °C. In this way, the target compounds (*R*)-**9i** and (*R*)-**9o** were obtained in 80 and 71% yield, respectively, and without erosion of enantiomeric purity. The synthesis of the enantiomer (*S*)-**9o** was also successfully accomplished starting from the adduct (*S*)-**3Ao**.

Conclusions

In summary, catalysts generated by combinations of Pd(TFA)$_2$ and pyridine–hydrazone ligands provide excellent enantiose-lectivities in the 1,2-addition of aryl boronic acids to formylphosphonate-derived hydrazones, yielding α-aryl α-hydra-zino phosphonates in high enantioselectivities (96 → 99% ee). Experimental evidence, DFT calculations and ASM-EDA analyses support a stereochemical model in which the hydrazone in its *Z*-configuration is coordinated to the aryl-palladium complex. The preferred transition state is not only stabilized by key non-covalent π···π and CH···π interactions between the hydrazone and the ligand, but also by significant electrostatic and orbital interactions, resulting in a remarkable enantiocontrol of the process. Moreover, the presence of a readily removable protect-ing group, such as Cbz in adducts **3**, has been exploited for tar-geting pyrazoles, phosphonopeptides and antitumoral hydrazide phosphonate oxadiazoles in enantiomerically pure forms, illus-trating the utility of the methodology.

Author contributions

D. M, J. M. L. and R. F. designed the project. S. A and J. R.-P. carried out experiments. I. F. performed computational studies and data analysis. D. M, J. M. L and I. F. wrote the manuscript – original draft. R. F: review and editing. All authors discussed the experimental results and commented on the manuscript.

Conflicts of interest

There are no conflicts to declare.

Acknowledgements

Notes and references

1 G. P. Horsman and D. L. Zechel, *Chem. Rev.*, 2017, **117**, 5704.

2 (*a*) J.-J. Shie, J.-M. Fang, P.-T. Lai, W.-H. Wen, S.-Y. Wang, Y.-S. E. Cheng, K.-C. Tsai, A.-S. Yang and C.-H. Wong, *J. Am. Chem. Soc.*, 2011, **133**, 17959; (*b*) J.-J. Shie, J.-M. Fang, S.-Y. Wang, K.-C. Tsai, Y.-S. E. Cheng, A.-S. Yang, S.-C. Hsiao, C.-Y. Su and C.-H. Wong, *J. Am. Chem. Soc.*, 2007, **129**, 11892; (*c*) P.-C. Wang, J.-M. Fang, K.-C. Tsai, S.-Y. Wang, W.-I. Huang, Y.-C. Tseng, Y.-S. E. Cheng, T.-J. R. Cheng and C.-H. Wong, *J. Med. Chem.*, 2016, **59**, 5297.

3 Y. Quin, R. Xing, S. Liu, H. Yu, K. Li, L. Hu and P. Li, *Int. J. Biol. Macromol.*, 2014, **63**, 83.

4 (*a*) D. Koszelewski, P. Kowalczyk, P. Śmigielski, J. Samsonowicz-Górski, K. Kramkowski, A. Wypych, M. Szymczak and R. Ostaszewski, *Materials*, 2022, **15**, 3846; (*b*) M. G. Nowak, A. S. Skwarecki and M. J. Milewska, *ChemMedChem*, 2021, **16**, 3513.

5 K. U. M. Rao, S. Swapna, D. M. Manidhar, K. M. K. Reddy and C. S. Reddy, *Phosphorus, Sulfur Silicon Relat. Elem.*, 2015, **190**, 232.

6 J. J. Uparkar, P. P. Dhavan, B. L. Jadhav and S. D. Pawar, *J. Iran. Chem. Soc.*, 2022, **19**, 3103.

7 S. Hkiri, M. Mekni-Toujani, E. Üstün, K. Hosni, A. Ghram, S. Touil, A. Samarat and D. Sémeril, *Pharmaceutics*, 2023, **15**, 114.

8 (*a*) Q. Wang, L. Yang, H. Ding, X. Chen, H. Wang and X. Tang, *Bioorg. Chem.*, 2016, **69**, 132; (*b*) F. Bahrami, F. Panahi, F. Daneshgar, R. Yousefi, M. B. Shahsavanib and A. Khalafi-Nezhad, *RSC Adv.*, 2016, **6**, 5915.

9 Reviews: (*a*) P. Kafarski and B. Lejczak, *Phosphorus, Sulfur Silicon Relat. Elem.*, 1991, **63**, 193; (*b*) A. Mucha, P. Kafarski and Ł. Berlicki, *J. Med. Chem.*, 2011, **54**, 5955; (*c*) M. Talma, M. Maślanka and A. Mucha, *Bioorg. Med. Chem. Lett.*, 2019, **29**, 1031; (*d*) For a review of the synthesis of enantioenriched derivatives see: P. R. Varga and G. Keglevich, *Molecules*, 2023, **28**, 6150.

10 (*a*) A. Aubry, J.-P. Mangeot, J. Vidal, A. Collet, S. Zerkout, M. Marraud and J. Pept, *Protein Res.*, 1994, **43**, 305; (*b*) T. Katoh and H. Suga, *J. Am. Chem. Soc.*, 2021, **143**, 18844.

11 E. F. Ewies, M. El-Hussieny, N. F. El-Sayed and M. A. Fouad, *Eur. J. Med. Chem.*, 2019, **180**, 310.

12 S. V. Tiwari, N. S. Sharif, R. I. Gajare, J. A. Seijas Vazquez, J. N. Sangshetti, M. D. Damale and A. P. G. Nikalje, *Molecules*, 2018, **23**, 1981.

13 L.-X. Xiao, K. Li, D.-Q. Shi and J. Heterocyclic, *Chem*, 2009, **46**, 555.

14 Pyrazolo[4,3-*e*][1,2,4]-triazolo[1,5-*d*]pyrimidines: L.-X. Xiao, K. Li and D.-Q. Shi, *Phosphorus, Sulfur Silicon Relat. Elem.*, 2008, **183**, 3156.

15 L. Bernardi, W. Zhuang and K. A. Jørgensen, *J. Am. Chem. Soc.*, 2005, **127**, 5772.

16 (*a*) N. Huang, X. Tong, S. Zhou, Q. Guo and Y. Peng, *Adv. Synth. Catal.*, 2019, **361**, 4805; (*b*) W. Wu, X. Yan, X. Li, Y. Ning, L. Hu, L. Zhu, Q. Ouyang and Y. Peng, *Org. Lett.*, 2022, **24**, 3766.

17 L.-P. Kong, N.-K. Li, S.-Y. Zhang, X. Chen, M. Zhao, Y.-F. Zhang and X.-W. Wang, *Org. Biomol. Chem.*, 2014, **12**, 8656.

18 N. S. Goulioukina, I. A. Shergold, V. B. Rybakov and I. P. Beletskaya, *Adv. Synth. Catal.*, 2017, **359**, 153.

19 (*a*) M. Velázquez, S. Alberca, J. Iglesias-Sigüenza, R. Fernández, J. M. Lassaletta and D. Monge, *Chem. Commun.*, 2020, **56**, 5823; (*b*) S. Alberca, M. Velázquez, J. Trujillo-Sierra, J. Iglesias-Sigüenza, R. Fernández,

J. M. Lassaletta and D. Monge, *Adv. Synth. Catal.*, 2022, **364**, 2373.

20 For a review of pyridine-oxazolines as chiral ligands for asymmetric catalysis, see: (*a*) G. Yang and W. Zhang, *Chem. Soc. Rev.*, 2018, **47**, 1783; Selected examples on asymmetric addition of organoboronic acids to C=N bonds:; (*b*) H. Dai, M. Yang and X. Lua, *Adv. Synth. Catal.*, 2008, **350**, 249; (*c*) J. Chen, X. Lu, W. Lou, Y. Ye, H. Jiang and W. Zeng, *J. Org. Chem.*, 2012, **77**, 8541; (*d*) G. Yang and W. Zhang, *Angew. Chem., Int. Ed.*, 2013, **52**, 7540; (*e*) M. Quan, G. Yang, F. Xie, I. D. Gridnev and W. Zhang, *Org. Chem. Front.*, 2015, **2**, 398; (*f*) M. Quan, X. Wang, L. Wu, I. D. Gridnev, G. Yang and W. Zhang, *Nat. Commun.*, 2018, **9**, 2258; (*g*) C. Jiang, Y. Lu and T. Hayashi, *Angew. Chem., Int. Ed.*, 2014, **53**, 9936.

21 (*a*) Y. Álvarez-Casao, D. Monge, E. Álvarez, R. Fernández and J. M. Lassaletta, *Org. Lett.*, 2015, **17**, 5104; (*b*) M. Retamosa, Y. Álvarez-Casao, E. Matador, A. Gómez, D. Monge, R. Fernández and J. M. Lassaletta, *Adv. Synth. Catal.*, 2019, **361**, 176. and reference 19.

22 J. I. Seeman, *Chem. Rev.*, 1983, **83**, 83–134.

23 P. Kaushik, B. Lai, C. D. Raghuveeran and R. Vaidyanathaswamy, *J. Org. Chem.*, 1982, **47**, 3503.

24 E. R. Johnson, S. Keinan, P. Mori-Sanchez, J. Contreras-Garcia, A. J. Cohen and W. Yang, *J. Am. Chem. Soc.*, 2010, **132**, 6498.

25 (*a*) I. Fernández and F. M. Bickelhaupt, *Chem. Soc. Rev.*, 2014, **43**, 4953; (*b*) L. P. Wolters and F. M. Bickelhaupt, *Wiley Interdiscip. Rev.: Comput. Mol. Sci.*, 2015, **5**, 324; (*c*) F. M. Bickelhaupt and K. N. Houk, *Angew. Chem., Int. Ed.*, 2017, **56**, 10070. See also;; (*d*) I. Fernández, in *Discovering the Future of Molecular Sciences* ed. B. Pignataro, Wiley-VCH, Weinheim, 2014, pp. 165–187.

26 For reviews on the EDA method, see: (*a*) F. M. Bickelhaupt and E. J. Baerends, in *Reviews in Computational Chemistry*, ed. K. B. Lipkowitz and D. B. Boyd, Wiley-VCH, New York, 2000, vol. 15, pp. 1–86; (*b*) M. von Hopffgarten and G. Frenking, *Wiley Interdiscip. Rev.: Comput. Mol. Sci.*, 2012, **2**, 43; (*c*) I. Fernández, in *Applied Theoretical Organic Chemistry*, ed. D. J. Tantillo, World Scientific, New Jersey, 2018, pp. 191–226.